

Critical Percolation Threshold for Solvation-Site Connectivity in Polymer Electrolyte Mixtures

Daniel Sharon, Chuting Deng, Peter Bennington, Michael A. Webb, Shrayesh N. Patel, Juan J. de Pablo,* and Paul F. Nealey*



Cite This: *Macromolecules* 2022, 55, 7212–7221



Read Online

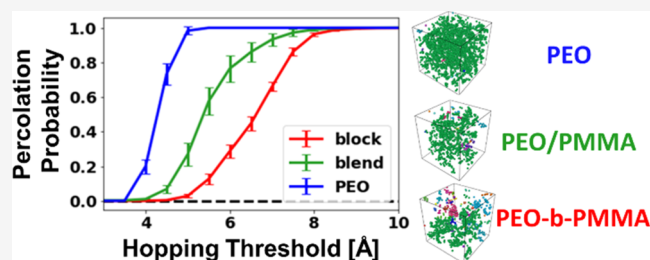
ACCESS |

Metrics & More

Article Recommendations

Supporting Information

ABSTRACT: Poly(ethylene oxide) (PEO)-based polymer electrolytes are often mixed with rigid, nonconductive polymers to improve mechanical strength. The suppressed conductivity of the mixture typically arises from a reduced segmental mobility and a diminished connectivity between conductive PEO sites. To decouple these two mechanisms, we compare transport in symmetric miscible blends and disordered block copolymers (BCP) of PEO and poly(methyl methacrylate) (PMMA). Because the two systems have identical physicochemical properties, differences in their conductivity directly reflect the underlying PEO network connectivity. We find that, at short distances ($<5 \text{ \AA}$), the Li^+ solvation networks are identical for the two systems; however, a distinct variation in the network connectivity arises at length scales between 5 and 10 \AA . Specifically, the BCP exhibits a lower connectivity, and therefore a lower conductivity than the blend. A quantitative model is proposed that associates long-range Li^+ transport with local miscibility; the concept of network connectivity discussed here could be useful for designing polymer electrolyte systems.



INTRODUCTION

To date, the most efficient polymer hosts for lithium-ion (Li^+) transport have been based on poly(ethylene oxide) (PEO).¹ The ionic transport mechanism in PEO-lithium bis(trifluoromethanesulfonyl)imide (LiTFSI) is based on the hopping of Li^+ between solvation sites composed of five to six ether oxygens (EO).^{2–4} The rate of hopping depends on the number of solvation sites, their connectivity, and segmental mobility.^{5–7} To achieve a reasonable conductivity, PEO must operate in its rubbery state, above its melting temperature, and well above its glass-transition temperature.⁸ This is because fast transport of Li^+ relies on fast chain motions of the polymer host, which only occur when the polymer material is in the rubbery state. Such transport improves as temperature increases. True solid-state battery applications, however, require a certain level of mechanical strength, which is believed to help suppress uncontrolled dendritic growth in Li-metal batteries.⁹ A common strategy to overcome this inherent trade-off between mechanical strength and ionic conductivity has been to mix PEO with a rigid, high- T_g polymer to form a robust solid electrolyte membrane. PEO-based blends can be formed through direct mixing (PEO/X)^{10–16} or by synthetic copolymerization (PEO-X),^{17–22} where X is a rigid component (X) that provides mechanical support but does not conduct Li^+ . While this mixed material could simultaneously achieve conductivity and mechanical integrity, it is often observed that improvements involve a compromise: the PEO phase within

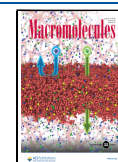
the mixture exhibits a lower ionic conductivity than the unmixed, pure material.^{22–26}

The addition of a glassy, nonconductive component reduces the conductivity of the mixed PEO phase through two main mechanisms. First, the low chain mobility of the glassy polymer component is believed to slow the segmental dynamics of the PEO domains in the mixture, thereby also slowing down Li^+ transport (which is tightly coupled to the chain mobility of the host). Recent studies have investigated how a contrast in host segmental dynamics affects the transport of Li^+ within it. Those studies considered Li^+ transport in poly(oligo-ethylene oxide) methacrylate (POEM), where flexible EO side chains are grafted onto glassy poly(methyl methacrylate) (PMMA) backbones.^{5,6} Reports indicate that the glassy backbone slows down the non-ion-solvating portion of the EO side chains and that the dynamics of the ion-solvating portions of the side chain are directly correlated with Li^+ mobility. Moreover, this body of research has shown that the PMMA backbone mixed into the system neither solvates nor conducts Li^+ . Instead, the very existence of nonconductive PMMA segments disrupts Li^+

Received: May 16, 2022

Revised: July 16, 2022

Published: August 11, 2022



transport pathways between conducting PEO sites (5–6 EO units). The “dilution” of conductive PEO segments by nonconductive polymeric components was originally identified by Mayes et al. as the second cause of lower ionic conductivity.²⁷

Only recently, with the refinement of the concept of solvation-site connectivity, have attempts been made to measure the diluting effect of nonconductive components.⁷ In some of these studies, the ionic conductivity of polymer electrolytes with different number and proximity of solvation sites (EO units) have been determined by means of extensive molecular dynamic (MD) simulations. The concept of solvation-site connectivity is gradually gaining favor, but questions remain about its importance relative to the effects of segmental mobility. Note that in most experimental systems, variations in the number or proximity of solvation sites lead to changes in the chemical (functional groups) and physical properties (segmental mobility) of the different electrolyte systems. As a result, quantification of the effects of solvation sites has been performed after artificially correcting for the chemical and physical disparities between the electrolyte systems. To overcome these shortcomings, in this work, we present a comparative study of symmetric blends and copolymers, where the chemical and physical properties of the electrolyte systems are the same, but the local solvation-site connectivity is different.

More specifically, we compare two types of polymer electrolyte mixtures based on PEO and poly(methyl methacrylate) (PMMA): a miscible polymer blend and a syntactic disordered block copolymer (BCP) PEO-*b*-PMMA. The mixtures have the same compositions (50:50 wt %) and are each blended with LiTFSI salt at the same concentrations ($r = [\text{Li}]/[\text{EO}] = 0.05$). Note that polymer mixtures based on PEO and PMMA are a good model system to investigate the relationship between ion transport and solvation-site connectivity for several reasons. First, as demonstrated by Lodge and McLeish, PEO, and PMMA mixtures are microscopically miscible, implying that chain conformations remain unaltered after mixing and do not adopt a particular long-range order.^{28,29} Second, it has been reported that PMMA as a dry homopolymer does not transport Li^+ ions. Therefore, the ionic conduction mechanism in the blend and BCP electrolytes relies on the PEO component and can be assumed to be identical to that of pure PEO. Third, as reported by Maranas et al., because the bulk segmental properties and chemical composition of the blend and BCP are identical, the only difference between the two systems should be the degree of mixing (miscibility) at length scales below 1.5 nm.³⁰ As a result, any changes in the ion transport behavior between them can be attributed to local changes in the connectivity of the PEO solvation-site network.

Our experimental measurements indicate that the ionic conductivity of the blend and the BCP systems is an order of magnitude lower than that of the unmixed PEO electrolyte. Furthermore, the ionic conductivity of the blend mixture is higher than that of the BCP electrolyte by a factor of 2. We propose that, in both blend and BCP systems, the presence of nonconducting PMMA near the PEO interferes with the ionic transport. Our simulation results corroborate this view and help establish a quantitative model that considers Li^+ transport between clusters, which are a direct result of PMMA mixing into PEO. These clusters occur at length scales of 5–10 Å, which are larger than the typical size of the immediate Li^+

solvation shell. In the context of polymer electrolyte mixtures, this newly acquired understanding of molecular packing, ion solvation behavior, and ion transport mechanism could help inform future design of nonhomogeneous polymer electrolyte systems.

■ MATERIALS

PEO (10 kg/mol), PMMA (11 kg/mol), and PEO-*b*-PMMA (11-11 kg/mol) were purchased from Polymer Source, Inc. and dried in an argon glovebox antechamber at 50 °C overnight before use. Acetonitrile (99.8%, anhydrous) was purchased from Sigma-Aldrich and used as received. Anhydrous LiTFSI was purchased from Sigma-Aldrich and was further dried under vacuum at 100 °C for 48 h. Polymers and LiTFSI were stored in an argon glovebox after the drying processes.

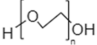
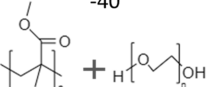
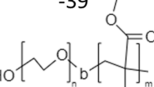
■ CHARACTERIZATION

Differential Scanning Calorimetry (DSC). Calorimetric glass-transition temperatures (T_g) of neat polymers and polymer electrolytes were determined by DSC using a TA Instruments Discovery 2500 DSC. Sample pans were prepared in the glovebox by drop-casting solutions, heating at 65 °C until dry, and then repeating until 5–10 mg of material was in the pan. The pans were then hermetically sealed before removing them from the glovebox to avoid any water adsorption before DSC measurement.

Vibrational Spectroscopy. Samples for Fourier transform infrared (FTIR) measurements were prepared on Au-coated Si substrates by spin coating. Samples were prepared inside a glovebox, annealed at 135 °C for 15 min, and sealed until immediately before measurement to minimize water absorption. Measurements were performed using a Shimadzu IRTracer-100 spectrometer using a diamond prism for attenuated total reflection (ATR) at ambient temperature from 400 to 4000 cm^{-1} .

Thin-Film Conductivity Measurements. Polymer electrolyte conductivity was determined by electrochemical impedance spectroscopy (EIS) of thin films on interdigitated electrodes (IDEs) as described previously.³¹ Briefly, IDEs are microfabricated by photolithography on top of thermal oxide Si wafers. Ti (5 nm) and then Au (45 nm) are deposited in the lithographically defined electrode area, and excess metal is removed by liftoff in warm *n*-methyl pyrrolidone. IDEs are designed with $N = 160$ electrodes, $l = 1$ mm of electrode overlap, $w = 2$ mm electrode width, and $d = 8$ mm interelectrode distance. Polymer electrolyte thin films were cast onto the IDEs by spin coating at 4000 rpm inside the glovebox, followed by drying on a hot plate at 70 °C before EIS measurements. Polymer film height (h) was determined by casting identical films on a Si wafer and performing ellipsometry (J.A. Woollam alpha-SE ellipsometer). Polymer films were in the range of 70–100 nm for this study. IDEs were placed on a custom heating stage in the glovebox and connected to a Gamry 600+ potentiostat by tungsten probe tips. Potentiostatic EIS was performed with an applied amplitude of 100 mV over a frequency range of 1 MHz–1 Hz. EIS data is fit to an appropriate equivalent circuit that models the physical process of thin films IDE systems using the Gamry E-chem Analyst software, and the resulting film resistance (R_f) is used to find the conductivity (σ) by eq 1. All conductivity data are reported as the average of three samples, with error bars representing the first standard deviation.

Table 1. Characteristics of Polymer Electrolyte Systems with LiTFSI ($r = 0.05$)

Characteristic	PEO	PEO/PMMA (50:50 wt. %)	PEO- <i>b</i> -PMMA
Mn / Kg·mol ⁻¹	10.0	10.0/11.5	11.0-11.0
T _g / °C	-50	-40	-39
Structure			

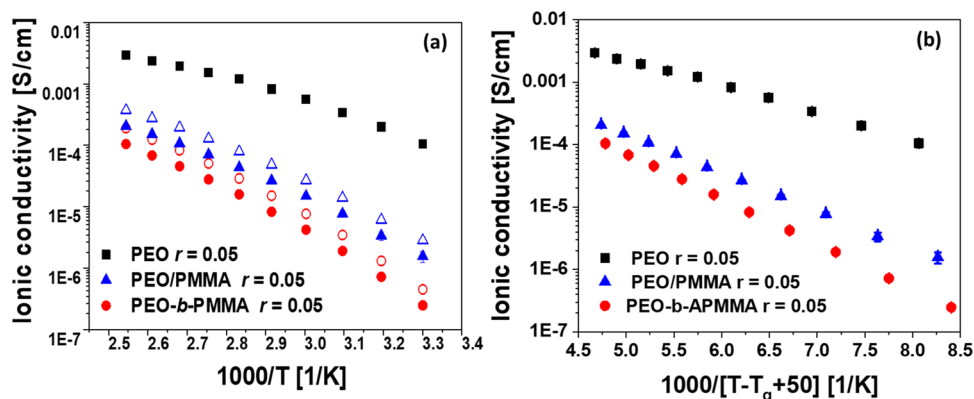


Figure 1. Polymer electrolyte ionic conductivity with LiTFSI ($r = 0.05$) as a function of (a) temperature and (b) temperature corrected by T_g ($T - T_g = 50$). In (a), the as-measured experimental conductivities are shown as solid symbols. The open symbols for mixed polymer electrolytes represent normalized conductivities by the volume fraction of PEO.

$$\sigma = \frac{d}{R_f(N-1)lh} \quad (1)$$

SIMULATION

In this study, the TraPPE-UA force field^{32–34} is used for all inter- and intramolecular interactions among polymer atoms. Compatible all-atom parameters for LiTFSI are adapted from a previous simulation study.³⁵ For all MD simulations, a cutoff radius of 12 Å with van der Waals tail correction is used for short-range Lennard–Jones (LJ) interactions. Long-range nonbonded interactions use a cutoff radius of 12 Å and are handled using the particle–particle particle–mesh solver with 10^{-4} accuracy.³⁶

The simulation is performed using the LAMMPS package.³⁷ The trajectories are integrated using the velocity-Verlet algorithm with a 1 fs timestep. For NVT simulations, the Nosé–Hoover thermostat with a damping parameter of 100 fs is used. For NPT simulations, the Nosé–Hoover barostat with a damping parameter of 1000 fs is applied in addition to the thermostat. Additional details of the simulation procedures and force field parameters are included in the [Supporting Information](#).

RESULTS AND DISCUSSION

As mentioned earlier, we examine experimentally and computationally two polymer electrolyte mixtures: (1) a miscible 50:50 wt % PEO/PMMA (10–11 kg/mol) blend electrolyte and (2) a disordered symmetric PEO-*b*-PMMA (11–11 kg/mol) BCP, both having a fixed LiTFSI concentration ($r = [\text{Li}]/[\text{EO}] = 0.05$). We begin by comparing the experimental ionic conductivity and simulated Li^+ transport of these two systems to those of a pure PEO-LiTFSI

(10 kg/mol) electrolyte having the same LiTFSI concentration (Table 1).

EIS measurements and equivalent circuits modeling were used to determine the resistivity of the polymer electrolytes that was then converted to ionic conductivity.³¹ The general assumption is that at relatively low concentrations like $r = 0.05$, majority of the TFSI anions are “free” and their motion is unaffected by the PEO conformation or coordination, whereas the Li cation is, and thus it is widely accepted to use ionic conductivity as a proxy to measure the Li^+ diffusivity. Figure 1a shows ionic conductivity as a function of temperature for PEO/PMMA blend, PEO-*b*-PMMA BCP, and PEO homopolymer electrolytes with LiTFSI ($r = 0.05$). At all temperatures, the ionic conductivity of the unmixed homopolymer electrolyte (PEO) exceeds that of the polymer mixtures by an order of magnitude. The conductivity of the disordered BCP is lower than that of the blend by a factor of two. Previous studies have shown that PMMA segments do not actively participate in the solvation or transport of Li^+ ;^{5,6} we therefore normalize the measured ionic conductivity by the PEO-LiTFSI volume fraction to account for the reduced Li^+ -conducting sites in the blend and BCP (Figure 1a, open symbols). Even after this normalization, the conductivities of the blend and BCP are still significantly lower than that of the unmixed PEO electrolyte. This finding implies that, while PMMA does not actively engage in the ion transport mechanism, its presence interferes with the passage of Li^+ through the PEO segments.

To understand why and how the presence of inactive fragments (PMMA) affects ionic transport within the blend and BCP electrolytes, we consider the two mechanisms mentioned in the introduction. First, the incorporation of high- T_g components, such as PMMA, tends to slow down the segmental mobilities of the material, which is essential to

promote Li^+ hopping in high-molecular-weight PEO-based electrolytes.^{24,38} To account for the conductivity differences due to the disparities in the segmental mobility (T_g), we further present the normalized conductivities as a function of reduced temperature, $T - T_g$ (Figure 1b). The addition of the glassy PMMA component increases the T_g of the mixtures by 10 °C (blend) and 11 °C (BCP) with respect to the unmixed PEO-LiTFSI system. The linear increase in ionic conductivity as a function of temperature corresponds to the VTF relationship, since the ionic transport in all samples is dependent on the segmental motion of the PEO chains. More importantly, we can observe that although the differences in ionic conductivities between the mixtures and the unmixed PEO-LiTFSI decrease after the T_g correction, the change is only minor. The conductivity difference between the blend and the BCP electrolyte is not affected by the correction either, as their T_g 's are virtually identical. Overall, T_g -normalized results show that while the reduction in segmental mobility is a valid explanation, it is not the major reason for the reduced conductivities observed here for the blend and BCP systems. The explanation for the lower ionic conductivity is most likely due to the second mechanism, in which the percolating PMMA segments disrupt (dilute) the solvation-site network formed by PEO segments. To examine that hypothesis, we next characterize the local miscibility (concentration fluctuation) of these systems at a molecular level.

Note that a common approach to assess miscibility in polymer blends is to characterize the glass transition behavior. The DSC curves of both the blend and the BCP electrolytes with $r = 0.05$ LiTFSI exhibit a singular glass transition at -41 and -39 °C, respectively. Generally, a single glass transition trace in DSC measurements indicates that the blend components are miscible. The measured T_g of the polymer electrolyte blend does not agree with the calculated T_g from the Fox equation for miscible binary blends ($T_{g\text{-fox}} \approx -23$ °C). Lodge and McLeish suggested that deviations from the Fox equation are caused by changes in the local concentration of the polymer components with respect to their bulk compositions.^{39,40} The origins of these changes can be intermolecular chain connectivity or concentration fluctuations.^{39–41} It was also suggested that in PEO/PMMA mixtures, the PEO has a measurable influence on PMMA mobility, whereas the presence of PMMA has a minor effect on PEO mobility until the matrix contains a sufficiently high concentration of PMMA (above 90%).⁴² This could explain why the T_g of our symmetric polymer electrolyte mixtures is more tilted toward the T_g of the PEO component. Our DSC measurements also reveal that such behavior is preserved after the addition of a Li salt ($r = 0.05$). To summarize, the DSC results indicate that the blend components are miscible and exhibit some asymmetry in their glass transition behavior. However, because their T_g 's are essentially the same, DSC measurements are insufficient to detect differences in local miscibility between the blend and the BCP, which might explain the difference in ionic conductivity.

While the glass transition provides a somewhat macroscopic account of polymeric blend miscibility, FTIR spectroscopy can be used to provide a measure of intermolecular interactions between the components of a mixture. Taking the spectra of the unmixed polymer components as a reference, changes in the FTIR spectra of the mixtures (such as peak decrease, shift, or broadening) can provide insights into structural changes at the molecular-level caused by the interaction or proximity

between different components.^{43,44} Figure 2 shows the FTIR spectra of the PEO/PMMA blend and the PEO-*b*-PMMA

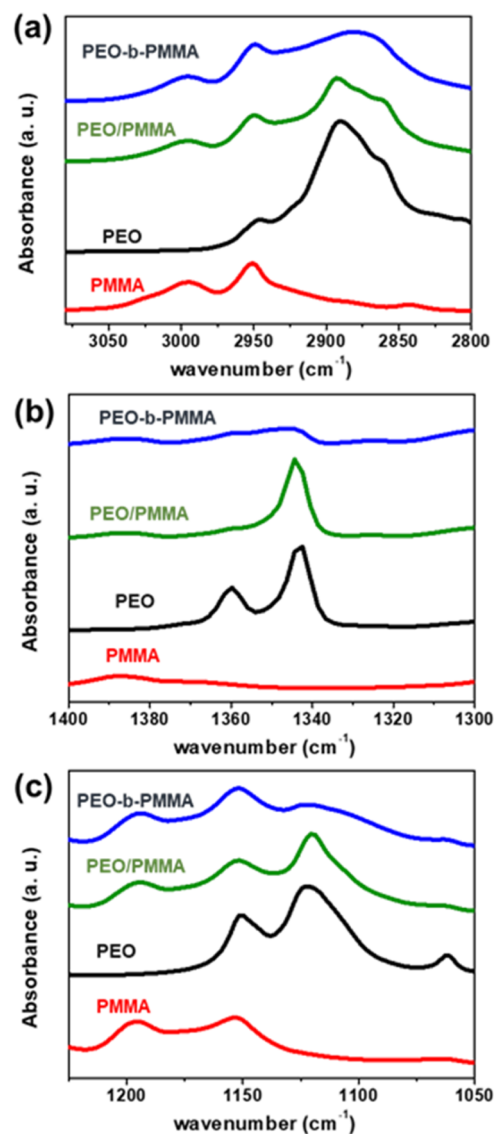


Figure 2. FTIR spectra of (a) CH_2 stretching, (b) CH_2 wagging, and (c) $\text{C}-\text{O}-\text{C}$ vibrations in the PEO/PMMA blend, the PEO-*b*-PMMA BCP, PEO homopolymer, and PMMA homopolymer.

BCP, along with those of the homopolymer PEO and PMMA for different wavenumber regions. Figure 2a focuses on the symmetric stretching of the PEO CH_2 groups, which is represented by multiple peaks in the range $2850\text{--}2900\text{ cm}^{-1}$. The PEO component in the PEO/PMMA blend does not present significant changes in the peak shape or height ratios. Conversely, the PEO-*b*-PMMA peak at 2891 cm^{-1} decreases considerably with respect to the unmixed PEO homopolymer. The same trend is observed for the characteristic CH_2 wagging vibration mode of the PEO component, where the decrease in the intensity of the sharp doublet at 1341 and 1360 cm^{-1} is more pronounced in the block copolymer sample (Figure 2b).⁴³ The PEO ether ($\text{C}-\text{O}-\text{C}$) vibration signature peaks between $1050\text{--}1150\text{ cm}^{-1}$ are presented in Figure 2c. The peaks at 1135 and 1057 cm^{-1} correspond to the crystalline PEO phase, while the peak centered around 1118 cm^{-1} includes both crystalline and amorphous phases. The

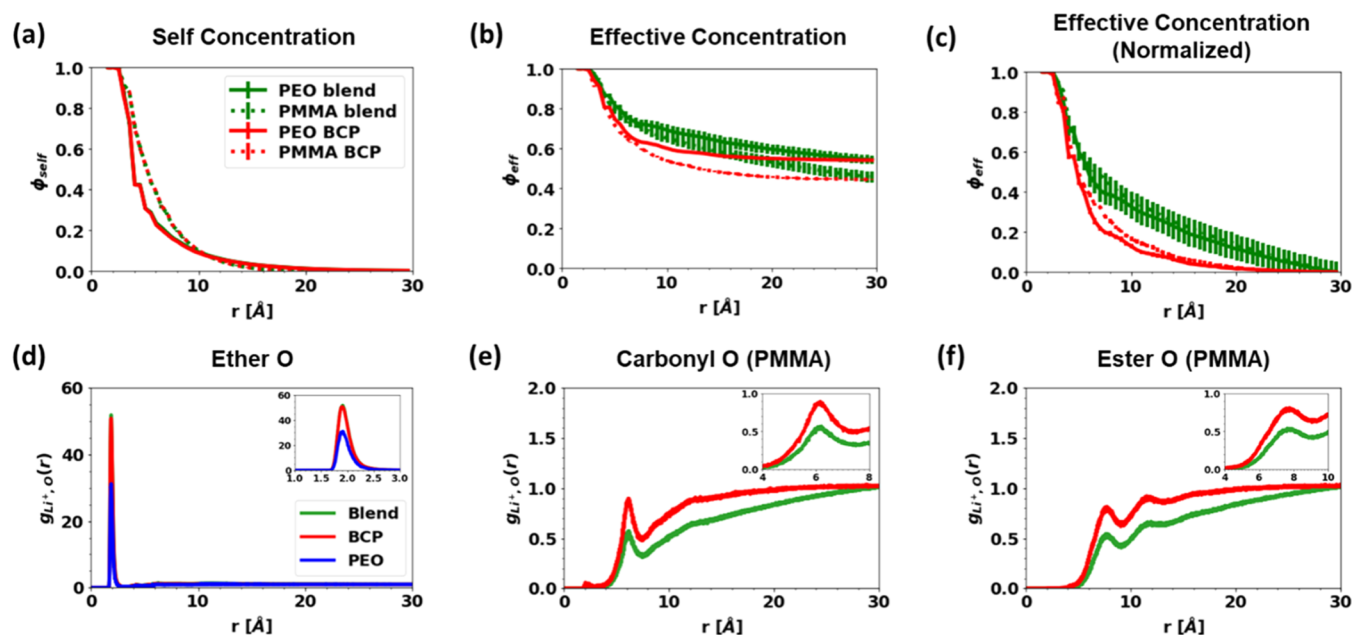


Figure 3. Li-oxygen radial distribution functions (RDF) for different oxygen types for the blend and BCP system. Note that the RDFs are normalized by the concentration of each oxygen type, so the relative heights of the peaks do not necessarily relate to the solvation shell composition.

crystalline PEO peaks in both mixtures are reduced with respect to the pure PEO; nonetheless, the decrease is more pronounced in the BCP sample. The suppression of the PEO crystalline phase by the introduction of a miscible polymer component has been well documented and can be attributed to the reduced formation of extended PEO chain crystals.⁴⁵ We found no evidence of any specific interactions between the two polymeric components, such as hydrogen bonding between the methyl ester PMMA hydrogens and the PEO ether oxygens or the PMMA carbonyl ester and the PEO hydrogens.⁴⁶ Nonetheless, we can observe that the PEO natural conformation is more disturbed in the BCP, which implies that the degree of miscibility in the BCP at a molecular level is higher than that in the blend. FTIR results are in good agreement with a previous simulation study by Maranas et al., where the local miscibility was suggested to be higher for the PEO-*b*-PMMA with respect to a blend.³⁰ In summary, we find that both mixtures are miscible, and the degree of miscibility for the BCP is higher than for the blend.

As noted above, there are two independent mechanisms by which ionic conduction in miscible polymer electrolyte mixtures can be reduced: glassy PMMA segments that slow down the PEO segmental motions, and a molecular “dilution” of the PEO fragments by the nonconductive PMMA component, leading to a disrupted EO network. In some polymer electrolyte mixtures, the overall reduced ionic transport is a combined effect of the two mechanisms. Here, however, we have shown that the segmental motion mechanism only accounts for a small portion of the difference in ionic conductivities between the mixtures and pure PEO, leading us to conclude that the dilution mechanism is the predominant contributor to the reduced ionic conductivity. In the following sections, we propose a model that helps explain the influence of the dilution effect on ionic conductivity.

Simulations of the PEO/PMMA blend and the BCP systems are particularly helpful for revealing the extent of local mixing of polymer segments and its influence on Li⁺ transport. The

results discussed in what follows were generated from three independent simulations at 190 K above the T_g of the corresponding system. Simulated T_g values and their calculations are included in the [Supporting Information](#). It is widely accepted that, in polymer electrolytes, the transport of Li⁺ relies on hopping between solvation sites, either along a polymer chain or from one chain to another.^{47,48} The solvation-site environment, i.e., the composition of solvation sites and the vicinity of available neighboring solvation sites, determines the hopping mechanism and the associated hopping rates.⁴⁹ We first consider the extent of miscibility via the concept of self- and effective concentrations^{30,39} (Figure 3a–c). The self-concentration decays from unity to zero and quantifies how closely a chain packs with itself; the effective concentration of a component decays from unity to its bulk volume fraction and indicates how closely a chain packs with other chains of the same species. Our results show that PEO and PMMA chains have identical intrachain packing in the blend and the BCP. However, the interchain packing of each component decays faster in the BCP, revealing a higher degree of intermixing in the BCP. Since the effective concentrations of PMMA and PEO decay to slightly different volume fractions (each is 50% by weight), we normalize the effective concentration to decay from unity to zero to provide a better visual comparison. The normalized results confirm the greater miscibility in the BCP relative to the blend. This finding is consistent with our FTIR measurements. A previous study reported similar inter- and intrachain packing behaviors for salt-free PEO/PMMA mixtures at a lower PEO content (20 wt %).³⁰ Our results extend that observation to systems that are more relevant for energy storage applications, i.e., mixtures with higher PEO content and with ions. To show how differences in polymer chain packing impact Li⁺ solvation, we describe the solvation environment using the pair radial distribution functions (RDFs) and oxygen atoms for the PEO (ether) and PMMA (carbonyl and ester) components (Figure 3d–f). We find that up to a radius of 4

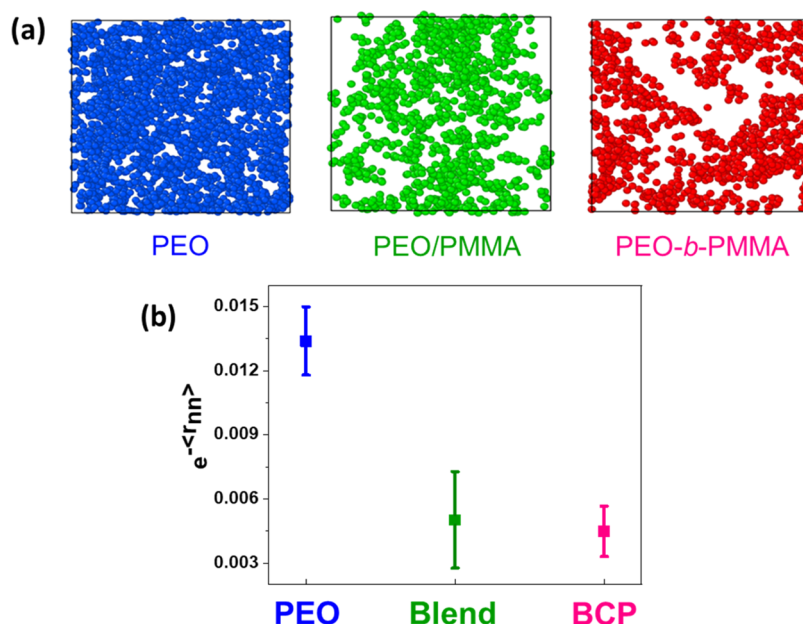


Figure 4. (a) Snapshots of viable solvation sites from the MD simulations. Viable solvation sites are shown as filled circles, where circle size reflects an approximate radius of 3.7 Å and the simulation boxes are approximately 60 Å in each dimension. (b) Average connectivity density for the different polymeric systems. The error bars derive from an averaging over 1000 snapshots.

Å, both blend and BCP systems show all-EO coordination is contributed by the PEO component, while PMMA oxygens only participate beyond $r \approx 6$ Å. The first solvation shell composition in the mixtures is identical to that in the unmixed PEO. Note that the RDFs are normalized by the concentration of the relevant atoms, so the decreased peak height of the first EO solvation peak in homopolymer PEO results from the normalization to a higher EO concentration in that system. Overall, it is of interest to note that the addition of PMMA to the mixtures does not alter the local solvation environment.

Since Li^+ ions are primarily solvated by EO units in both the blend and BCP systems and in PEO, we can infer that their conductivity relies on the same ionic transport mechanism, i.e., hopping between sites formed by ether oxygens only. Therefore, the Li^+ transport models presented in what follows for miscible polymer mixtures share the same criteria for identifying viable solvation sites as used in a series of PEO-based homopolymer hosts.^{5,6,49,50}

Here, we adopt the solvation-site connectivity protocol by Webb et al. but in the context of miscible polymer mixtures.⁷ Specifically, a viable solvation site in a PEO-based electrolyte is defined at the centroid of a set of five or more EO atoms, each within 3.7 Å of the centroid. Figure 4a shows representative snapshots of viable solvation sites for the homopolymer, the blend, and the BCP electrolyte systems at a salt concentration of $r = 0.05$. Visually, both miscible mixture electrolytes appear to have fewer viable solvation sites than the unmixed PEO electrolyte. Furthermore, while solvation sites tend to organize into isolated clusters in the mixtures, they are evenly distributed in the PEO electrolyte, where they form a well-connected network. To quantitatively compare the different systems, we compute the solvation-site connectivity defined as $\kappa = \exp(-\langle r_{nn} \rangle)$, where $\langle r_{nn} \rangle$ is the average nearest neighbor distance.⁷ As shown in Figure 4b, the connectivity in PEO appears to be more than 3 times higher than in the blend and BCP systems. Although the difference in connectivity is less dramatic than the factor of ten difference between the

conductivity of PEO and the mixed electrolyte systems, it demonstrates that the addition of PMMA suppresses Li^+ conduction mainly by diluting and disrupting the solvation-site network. Solvation-site connectivity, however, does not reveal a difference between the blend and the BCP. Recall that the blend exhibits a conductivity that is twice as large as that of the BCP.

We next consider the length scale at which the solvation-site connectivity describes the solvation-site network. As described here and in previous studies, the solvation-site connectivity is proportional to the characteristic hopping rate between two solvation sites separated by $\langle r_{nn} \rangle$. The logic behind this approach originates from a transition state-like theory, where the rate or likelihood of a hopping event is inversely related to its energy barrier, which we assume to increase linearly with the distance between sites. Because the hopping rate decays exponentially as the distance increases, the connectivity metric is dominated by short-range Li^+ hopping events that occur at the length scale of the immediate solvation environment (within 5 Å), and it only incorporates limited information about how solvation sites are arranged on a larger length scale. When comparing the blend and the BCP, the immediate solvation environment is identical in the two systems, and the most critical difference between them lies in the molecular packing at length scales in the range of 5–10 Å, where miscibility heterogeneity is manifest. An effective model for ion transport in these systems must therefore highlight features of the solvation-site network at such length scales.

To better quantify the long-range connectivity of solvation sites, we first apply a percolation analysis. First, we group solvation sites into ionic conductive clusters. Under the context of ion hopping between solvation sites, we assumed that a Li^+ could hop from one solvation site to another when the distance between them is lower than a given hopping threshold d . If two sites are separated by a distance larger than the threshold, they are considered disconnected and can be defined as isolated clusters. Figure 5a displays representative snapshots of

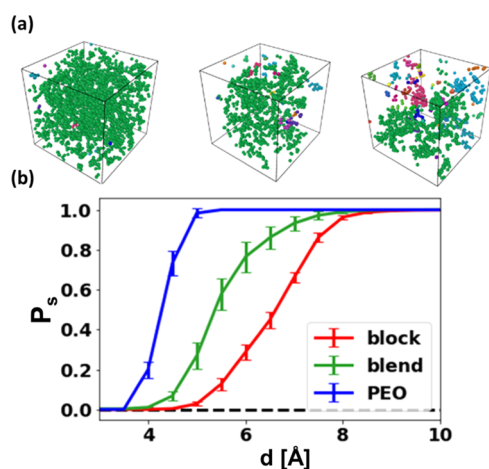


Figure 5. (a) Representative configurations of percolated clusters with cutoff length of 6 Å and (b) percolation probability plotted as a function of normalized edge length cutoff.

solvation-site clusters at a representative hopping threshold distance $d = 6$ Å. Different colors represent isolated clusters that are separated by at least 6 Å from one another. We find that, in the unmixed PEO, solvation sites form an overall connected network, where almost all solvation sites belong to the same cluster. In contrast, in the blend and the BCP systems, the solvation sites aggregate into a few isolated clusters instead of forming a single connected cluster. The BCP system appears to have more isolated clusters than the blend. To characterize how the formation of clusters disrupts the network of solvation sites, we follow a similar idea and examine the spanning percolation probability (P_s) as a function of hopping threshold (d) to identify the critical length scale for percolation transitions. The term spanning probability defines the likelihood that a solvation-site cluster is connected across the ~ 60 Å simulation box along at least one of the three Cartesian directions. Figure 5b presents the calculated P_s as a function of d in the unmixed PEO, the blend, and the BCP. Because P_s is averaged over 1000 frames of different fluctuating solvation-site configurations, the percolation transition in each system exhibits a smooth curve, instead of a step function, growing from zero to unity as d increases. We find that the largest difference between unmixed PEO and the mixtures occurs at approximately 4.5 Å, which is roughly the size of the second solvation shell, and therefore reflects the nearest neighbor distance. This implies that in the unmixed PEO, long-range Li^+ transport occurs as long as short-range transport, i.e., hopping from one site to its immediate neighbor, is enabled. For the mixture systems, however, this is not the case; short-range transport only allows a Li^+ to move within a cluster, but not across isolated clusters. In other words, in PEO the rate-limiting process for long-range transport is intersolvation-site transport, while in the mixtures, it is intercluster transport. A comparison of the blend and the BCP shows that their P_s differ most significantly at $d \sim 6$ Å. Recall that the local effective concentrations also exhibit the largest difference at around ~ 6 Å (Figure 3a). Based on these findings, we attribute the greater disruption in the solvation-site network observed in the BCP to its higher degree of mixing, or lower local effective concentration of PEO units at that length scale. These results confirm that the key intermediate-range features of the underlying solvation-site network are determined by molecular arrangements at length scales of 5–10 Å and that this critical

length regime is larger than that considered in the original solvation-site connectivity model. Note that the cutoff distances identified here do not correspond to previously reported ionic transport mechanisms, but they can be used to highlight critical length scales that might affect ionic transport efficiency in mixed polymer electrolyte systems.

The relevance of solvation-site cluster connectivity can be better understood by introducing a different transport model. We do so by applying the Kirchoff transport index (K_T) as described by Jackson and co-workers, which was shown to be successful in quantifying charge transport in bulk organic photovoltaic materials.⁵¹ That classical resistance theory is adapted here to analyze Li^+ transport in the solvation-site network. In a network of solvation sites, the “admittance” between two sites is related to the probability of hopping, P_{hop} , which is expressed as a function of the separation distance r , $P_{\text{hop}} \propto e^{-r}$. K_T is defined as the normalized sum of the inverse resistance distances between every pair of solvation sites. For additional details, readers are referred to Jackson et al.’s original work.⁵¹ Figure 6 presents the calculated K_T for each

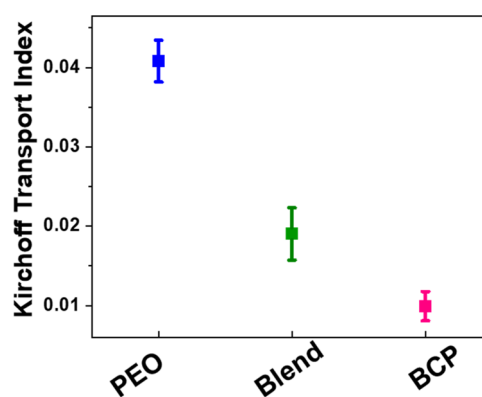


Figure 6. Kirchoff transport indices K_T for studied ionic transport in polymer electrolyte systems.

system. We find that K_T in the blend is 2 times higher than in the BCP, which is consistent with the factor of two reported here in their ionic conductivities. Comparing the mixtures to the unmixed PEO, K_T does not reproduce the factor of ten difference in conductivity; K_T seems to only capture the relative difference in ionic conductivity due to the degree of miscibility in the blend and BCP systems. In contrast to the solvation-site connectivity, which is solely based on nearest neighbor distances, K_T considers all possible pairwise distances between viable solvation sites and assigns to them a relative importance. This model not only considers short-range transport between neighboring sites but also accounts for the long-range transport involving Li^+ transport between solvation-site clusters. While the relative contributions from intra- and intercluster transport might not be captured quantitatively, we believe this model is useful for the analysis of transport in mixed systems.

As noted above, this model determines resistance distances between pairs of solvation sites regardless of how far they are. However, long-range ion hopping events between clusters that are more than 6 Å apart are unlikely. Actual ion hopping events occur between neighboring solvation sites, and the transport between clusters possibly relies on their rearrangement. One should therefore evaluate the segmental dynamics, which is closely associated with the rate of rearrangement of solvation

sites and solvation-site clusters.⁵⁰ Here, we argue that for comparable chain dynamics, the time required for solvation-site rearrangement is proportional to the length scale of the rearrangement. This is the case in our study, where the segmental dynamics are comparable for the blend and the BCP systems so that differences in the spatial arrangement of solvation sites directly explain differences in conductivity. Also note that the model originally intended for electron transport assumes that the transport between nodes is much faster than the rearrangement of the network. That might not be the case for Li⁺ hopping in PEO,⁵⁰ and this model merely highlights how the critical length scale of a time-averaged, static representation of solvation-site networks can be connected to the rate of Li⁺ transport.

The critical length scales identified here provide a first step toward understanding Li⁺ transport in polymer electrolyte mixtures. To arrive at a complete physical picture, it is necessary to also evaluate and consider the kinetics of the rate-limiting mechanisms for long-range Li⁺ transport. In this work, we have shown that in PEO the intersolvation-site hopping is rate-limiting, and it depends on segmental relaxations at a length scale below 5 Å. In the blend and BCP systems, the rate-limiting process is the intercluster transport, which depends on segmental relaxations at length scales in the 5–10 Å range. For these different rate-limiting processes, the need for relaxation at a larger length scale is further linked to a higher activation energy, which could manifest in a more dramatic temperature dependence. We are currently developing a time-temperature superposition principle to investigate Li⁺ transport behavior for a dynamic representation of solvation-site networks. The goal is to elucidate the underlying kinetics by determining the time scale for Li⁺ hopping events relative to that of solvation network rearrangement as a function of temperature.

CONCLUSIONS

The comparison of Li⁺ transport in homopolymer PEO and PEO-containing polymer blends and BCP electrolytes presented here helps explain several physical processes that influence conductivity. These materials exhibit essentially identical thermophysical properties and only differ by their local concentration conditions. Experimental characterization and MD simulations reveal that the critical percolation threshold for Li⁺ transport is closely associated with local miscibility features that arise at length scales in the 5–10 Å range.

Our experiments indicate that the ionic conductivity of the blend and the BCP is an order of magnitude lower than that of the unmixed PEO electrolyte. Further, the ionic conductivity of the blend is higher than that of the BCP electrolyte by a factor of two. The PMMA near the PEO interferes with ionic transport, as revealed by our observation that the BCP, which has a higher degree of miscibility than the blend, exhibits a greater reduction in ionic conductivity.

Our simulation results provide a quantitative framework to understand the proposed mechanism. Simulated effective concentrations confirm that the BCP is more homogeneous than the blend and that the miscibility difference between the two mixtures is most apparent in changes in the local concentration at length scales of 5–10 Å. The first Li⁺ solvation shell in the mixtures is similar to that in the pure PEO. Between the blends and the BCP, the miscibility difference causes the Li⁺ solvation environment to differ only after 6 Å. A cluster analysis confirms that the critical length

scale at which the presence of PMMA near PEO can affect Li⁺ transport efficiency is approximately 6 Å. The spanning probability analysis confirms that the rate-limiting process for long-range Li⁺ transport is the intersolvation-site hopping (<5 Å) in PEO and intercluster transport (5–10 Å) in the mixtures. These views were further substantiated by combining a solvation-site connectivity analysis κ and introducing a Kirchoff transport index K_T to model Li⁺ transport in blends and BCP systems. The first model captures the relative conductivity difference between pure PEO and the mixed electrolytes, but it does not differentiate between the blend and the BCP. We believe this is due to different degrees of solvation-site clustering in the mixture and BCP at length scales of 5–10 Å. The second model successfully captures the nuanced conductivity difference, caused by the degree of miscibility between the two systems. The model considers Li⁺ transport within and between clusters, where the latter is a direct result of PMMA mixing into PEO and occurs at length scales longer that extend beyond the typical size of the first Li⁺ solvation shell. This newly acquired understanding of molecular packing, ion solvation behavior, and ion transport model in the context of polymer electrolyte mixtures could help inform future design of combined polymer electrolyte systems.

ASSOCIATED CONTENT

Supporting Information

The Supporting Information is available free of charge at <https://pubs.acs.org/doi/10.1021/acs.macromol.2c00988>.

Additional experimental figures; simulation force field and protocols; and additional simulation figures (PDF)

AUTHOR INFORMATION

Corresponding Authors

Juan J. de Pablo – Pritzker School of Molecular Engineering, University of Chicago, Chicago, Illinois 60637, United States; Materials Science Division, Argonne National Laboratory, Lemont, Illinois 60439, United States; orcid.org/0000-0002-3526-516X; Email: depablo@uchicago.edu

Paul F. Nealey – Pritzker School of Molecular Engineering, University of Chicago, Chicago, Illinois 60637, United States; Materials Science Division, Argonne National Laboratory, Lemont, Illinois 60439, United States; orcid.org/0000-0003-3889-142X; Email: nealey@uchicago.edu

Authors

Daniel Sharon – Institute of Chemistry, The Hebrew University of Jerusalem, Jerusalem 91904, Israel; orcid.org/0000-0002-3385-1536

Chuting Deng – Pritzker School of Molecular Engineering, University of Chicago, Chicago, Illinois 60637, United States; orcid.org/0000-0002-0416-178X

Peter Bennington – Pritzker School of Molecular Engineering, University of Chicago, Chicago, Illinois 60637, United States; orcid.org/0000-0002-0501-1441

Michael A. Webb – Department of Chemical and Biological Engineering, Princeton University, Princeton, New Jersey 08540, United States; orcid.org/0000-0002-7420-4474

Shrayesh N. Patel – Pritzker School of Molecular Engineering, University of Chicago, Chicago, Illinois 60637, United States; orcid.org/0000-0003-3657-827X

Complete contact information is available at:

<https://pubs.acs.org/10.1021/acs.macromol.2c00988>

Author Contributions

The manuscript was written through contributions of all authors. The authors declare no competing financial interest.

Notes

The authors declare no competing financial interest.

ACKNOWLEDGMENTS

The authors gratefully acknowledge support by the U.S. Department of Energy (DOE), Basic Energy Sciences, Materials Sciences, and Engineering Division. This work made use of the Pritzker Nanofabrication Facility, which receives partial support from the SHyNE Resource, a node of the National Science Foundation's National Nanotechnology Coordinated Infrastructure (NSF ECCS-2025633). This work made use of the shared facilities at the University of Chicago Materials Research Science and Engineering Center, supported by National Science Foundation under award number DMR-2011854. Parts of this work were carried out at the Soft Matter Characterization Facility of the University of Chicago. The simulations were completed on computational resources provided by the University of Chicago Research Computing Center. M.A.W. acknowledges support from Princeton University.

REFERENCES

- (1) Xue, Z.; He, D.; Xie, X. Poly(Ethylene Oxide)-Based Electrolytes for Lithium-Ion Batteries. *J. Mater. Chem. A* **2015**, *3*, 19218–19253.
- (2) Borodin, O.; Smith, G. D. Mechanism of Ion Transport in Amorphous Poly(Ethylene Oxide)/LiTFSI from Molecular Dynamics Simulations. *Macromolecules* **2006**, *39*, 1620–1629.
- (3) Borodin, O.; Smith, G. D. Molecular Dynamics Simulations of Poly(Ethylene Oxide)/LiI Melts. I. Structural and Conformational Properties. *Macromolecules* **1998**, *31*, 8396–8406.
- (4) Diddens, D.; Heuer, A.; Borodin, O. Understanding the Lithium Transport within a Rouse-Based Model for a PEO / LiTFSI Polymer Electrolyte. *Macromolecules* **2010**, *43*, 2028–2036.
- (5) Bennington, P.; Deng, C.; Sharon, D.; Webb, M. A.; de Pablo, J. J.; Nealey, P. F.; Patel, S. N. Role of Solvation Site Segmental Dynamics on Ion Transport in Ethylene-Oxide Based Side-Chain Polymer Electrolytes. *J. Mater. Chem. A* **2021**, *9*, 9937–9951.
- (6) Deng, C.; Webb, M. A.; Bennington, P.; Sharon, D.; Nealey, P. F.; Patel, S. N.; de Pablo, J. J. Role of Molecular Architecture on Ion Transport in Ethylene Oxide-Based Polymer Electrolytes. *Macromolecules* **2021**, *54*, 2266–2276.
- (7) Pesko, D. M.; Webb, M. A.; Jung, Y.; Zheng, Q.; Miller, T. F.; Coates, G. W.; Balsara, N. P. Universal Relationship between Conductivity and Solvation-Site Connectivity in Ether-Based Polymer Electrolytes. *Macromolecules* **2016**, *49*, 5244–5255.
- (8) Lascaud, S.; Perrier, M.; Vallée, A.; Besner, S.; Prud'homme, J.; Armand, M. Phase Diagrams and Conductivity Behavior of Poly-(Ethylene Oxide)-Molten Salt Rubbery Electrolytes. *Macromolecules* **1994**, *27*, 7469–7477.
- (9) Barai, P.; Higa, K.; Srinivasan, V. Lithium Dendrite Growth Mechanisms in Polymer Electrolytes and Prevention Strategies. *Phys. Chem. Chem. Phys.* **2017**, *19*, 20493–20505.
- (10) Abdul Halim, S. I.; Chan, C. H.; Kressler, J. Effects on the Properties after Addition of Lithium Salt in Poly(Ethylene Oxide)/Poly(Methyl Acrylate) Blends. *Polymers* **2020**, *12*, 2963.
- (11) Yap, Y. L.; You, A. H.; Teo, L. L. Preparation and Characterization Studies of PMMA-PEO-Blend Solid Polymer Electrolytes with SiO₂ Filler and Plasticizer for Lithium Ion Battery. *Ionics* **2019**, *25*, 3087–3098.
- (12) Tao, C.; Gao, M. H.; Yin, B. H.; Li, B.; Huang, Y. P.; Xu, G.; Bao, J. J. A Promising TPU/PEO Blend Polymer Electrolyte for All-Solid-State Lithium Ion Batteries. *Electrochim. Acta* **2017**, *257*, 31–39.
- (13) Jeddi, K.; Qazvini, N. T.; Jafari, S. H.; Khonakdar, H. A. Enhanced Ionic Conductivity in PEO / PMMA Glassy Miscible Blends: Role of Nano-Confinement of Minority Component Chains. *J. Polym. Sci., Part B: Polym. Phys.* **2010**, *48*, 2065–2071.
- (14) Osman, Z.; Anzor, N. M.; Chew, K. W.; Kamarulzaman, N. Infrared and Conductivity Studies on Blends of PMMA/PEO Based Polymer Electrolytes. *Ionics* **2005**, *11*, 431–435.
- (15) Florjańczyk, Z.; Such, K.; Wiczorek, W.; Wasiucionek, M. Highly Conductive Poly(Ethylene Oxide)-Poly(Methyl Methacrylate) Blends Complexed with Alkali Metal Salts. *Polymer* **1991**, *32*, 3422–3425.
- (16) Florjańczyk, Z.; Such, K.; Wiczorek, W. Effect of Tacticity of Poly(Methyl Methacrylate) on Conductivity of Poly(Ethylene Oxide)-Poly(Methyl Methacrylate) Blend-Based Polymeric Electrolyte. *J. Macromol. Sci., Part A* **1992**, *29*, 853–863.
- (17) Young, W. S.; Albert, J. N. L.; Schantz, A. B.; Epps, T. H. Mixed-Salt Effects on the Ionic Conductivity of Lithium-Doped PEO-Containing Block Copolymers. *Macromolecules* **2011**, *44*, 8116–8123.
- (18) Young, W.-S.; Kuan, W.-F.; Epps, T. H. Block Copolymer Electrolytes for Rechargeable Lithium Batteries. *J. Polym. Sci., Part B: Polym. Phys.* **2014**, *52*, 1–16.
- (19) Maslyn, J. A.; Frenck, L.; Loo, W. S.; Parkinson, D. Y.; Balsara, N. P. Extended Cycling through Rigid Block Copolymer Electrolytes Enabled by Reducing Impurities in Lithium Metal Electrodes. *ACS Appl. Energy Mater.* **2019**, *2*, 8197–8206.
- (20) Chintapalli, M.; Chen, X. C.; Thelen, J. L.; Teran, A. A.; Wang, X.; Garetz, B. A.; Balsara, N. P. Effect of Grain Size on the Ionic Conductivity of a Block Copolymer Electrolyte. *Macromolecules* **2014**, *47*, 5424–5431.
- (21) Schauer, N. S.; Harry, K. J.; Parkinson, D. Y.; Watanabe, H.; Balsara, N. P. Lithium Dendrite Growth in Glassy and Rubbery Nanostructured Block Copolymer Electrolytes. *J. Electrochem. Soc.* **2015**, *162*, A398–A405.
- (22) Irwin, M. T.; Hickey, R. J.; Xie, S.; So, S.; Bates, F. S.; Lodge, T. P. Structure-Conductivity Relationships in Ordered and Disordered Salt-Doped Diblock Copolymer/Homopolymer Blends. *Macromolecules* **2016**, *49*, 6928–6939.
- (23) Xie, S.; Meyer, D. J.; Wang, E.; Bates, F. S.; Lodge, T. P. Structure and Properties of Bicontinuous Microemulsions from Salt-Doped Ternary Polymer Blends. *Macromolecules* **2019**, *52*, 9693–9702.
- (24) Bouchet, R.; Phan, T. N. T.; Beaudoin, E.; Devaux, D.; Davidson, P.; Bertin, D.; Denoyel, R. Charge Transport in Nanostructured PS-PEO-PS Triblock Copolymer Electrolytes. *Macromolecules* **2014**, *47*, 2659–2665.
- (25) Sharon, D.; Bennington, P.; Dolejsi, M.; Webb, M. A.; Dong, B. X.; de Pablo, J. J.; Nealey, P. F.; Patel, S. N. Intrinsic Ion Transport Properties of Block Copolymer Electrolytes. *ACS Nano* **2020**, *14*, 8902–8914.
- (26) Glynos, E.; Petropoulou, P.; Mygiakis, E.; Nega, A. D.; Pan, W.; Papoutsakis, L.; Giannelis, E. P.; Sakellariou, G.; Anastasiadis, S. H. Leveraging Molecular Architecture to Design New, All-Polymer Solid Electrolytes with Simultaneous Enhancement in Modulus and Ionic Conductivity. *Macromolecules* **2018**, *51*, 2542–2550.
- (27) Ruzette, A.-V. G.; Soo, P. P.; Sadoway, D. R.; Mayes, A. M. Melt-Formable Block Copolymer Electrolytes for Lithium Rechargeable Batteries. *J. Electrochem. Soc.* **2001**, *148*, A537–A543.
- (28) Mu, D.; Huang, X. R.; Lu, Z. Y.; Sun, C. C. Computer Simulation Study on the Compatibility of Poly(Ethylene Oxide)/Poly(Methyl Methacrylate) Blends. *Chem. Phys.* **2008**, *348*, 122–129.
- (29) Dionísio, M.; Fernandes, A. C.; Mano, J. F.; Correia, N. T.; Sousa, R. C. Relaxation Studies in PEO/PMMA Blends. *Macromolecules* **2000**, *33*, 1002–1011.
- (30) Sacristan, J.; Chen, C.; Maranas, J. K. Role of Effective Composition on Dynamics of PEO-PMMA Blends. *Macromolecules* **2008**, *41*, 5466–5476.

(31) Sharon, D.; Bennington, P.; Liu, C.; Kambe, Y.; Dong, B. X.; Burnett, V. F.; Dolejsi, M.; Grocke, G.; Patel, S. N.; Nealey, P. F. Interrogation of Electrochemical Properties of Polymer Electrolyte Thin Films with Interdigitated Electrodes. *J. Electrochem. Soc.* **2018**, *165*, H1028–H1039.

(32) Martin, M. G.; Siepmann, J. I. Transferable Potentials for Phase Equilibria. 1. United-Atom Description of n-Alkanes. *J. Phys. Chem. B* **1998**, *102*, 2569–2577.

(33) Stubbs, J. M.; Potoff, J. J.; Siepmann, J. I. Transferable Potentials for Phase Equilibria. 6. United-Atom Description for Ethers, Glycols, Ketones, and Aldehydes. *J. Phys. Chem. B* **2004**, *108*, 17596–17605.

(34) Maerzke, K. A.; Schultz, N. E.; Ross, R. B.; Siepmann, J. I. TraPPE-UA Force Field for Acrylates and Monte Carlo Simulations for Their Mixtures with Alkanes and Alcohols. *J. Phys. Chem. B* **2009**, *113*, 6415–6425.

(35) Canongia Lopes, J. N.; Pascal, B. Molecular Force Field for Ionic Liquids Composed of Triflate or Bistriflylimide Anions. *J. Chem. Phys. B* **2004**, *108*, 16893–16898.

(36) Brown, W. M.; Kohlmeyer, A.; Plimpton, S. J.; Tharrington, A. N. Implementing Molecular Dynamics on Hybrid High Performance Computers – Particle–Particle Particle-Mesh. *Comput. Phys. Commun.* **2012**, *183*, 449–459.

(37) Plimpton, S. Fast Parallel Algorithms for Short-Range Molecular Dynamics. *J. Comput. Phys.* **1995**, *117*, 1–19.

(38) Huynh, T. V.; Messinger, R. J.; Sarou-Kanian, V.; Fayon, F.; Bouchet, R.; Deschamps, M. Restricted Lithium Ion Dynamics in PEO-Based Block Copolymer Electrolytes Measured by High-Field Nuclear Magnetic Resonance Relaxation. *J. Chem. Phys.* **2017**, *147*, No. 134902.

(39) Lodge, T. P.; McLeish, T. C. B. Self-Concentrations and Effective Glass Transition Temperatures in Polymer Blends. *Macromolecules* **2000**, *33*, 5278–5284.

(40) Gaikwad, A. N.; Wood, E. R.; Ngai, T.; Lodge, T. P. Two Calorimetric Glass Transitions in Miscible Blends Containing Poly(Ethylene Oxide). *Macromolecules* **2008**, 2502–2508.

(41) Zawada, J. A.; Ylitalo, C. M.; Fuller, G. G.; Colby, R. H.; Long, T. E. Component Relaxation Dynamics in a Miscible Polymer Blend: Poly(Ethylene Oxide)/Poly(Methyl Methacrylate). *Macromolecules* **1992**, *25*, 2896–2902.

(42) Zeroni, I.; Ozair, S.; Lodge, T. P. Component Terminal Dynamics in Poly(Ethylene Oxide)/Poly(Methyl Methacrylate) Blends. *Macromolecules* **2008**, *41*, 5033–5041.

(43) Chiu, C.-Y.; Chen, H.; Kuo, S.; Huang, C.; Chang, F.-C. Investigating the Effect of Miscibility on the Ionic Conductivity of LiClO₄/PEO/PCL Ternary Blends. *Macromolecules* **2004**, *37*, 8424–8430.

(44) Ravindar Reddy, M.; Subrahmanyam, A. R.; Maheshwar Reddy, M.; Siva Kumar, J.; Kamalaker, V.; Jaipal Reddy, M. X-RD, SEM, FT-IR, DSC Studies of Polymer Blend Films of PMMA and PEO. *Mater. Today: Proc.* **2016**, *3*, 3713–3718.

(45) Pfefferkorn, D.; Kyeremateng, S. O.; Busse, K.; Kammer, H. W.; Thurn-Albrecht, T.; Kressler, J. Crystallization and Melting of Poly(Ethylene Oxide) in Blends and Diblock Copolymers with Poly(Methyl Acrylate). *Macromolecules* **2011**, *44*, 2953–2963.

(46) Abutalib, M. M.; Rajeh, A. Influence of Fe₃O₄ Nanoparticles on the Optical, Magnetic and Electrical Properties of PMMA/PEO Composites: Combined FT-IR/DFT for Electrochemical Applications. *J. Organomet. Chem.* **2020**, *920*, No. 121348.

(47) Hallinan, D. T., Jr; Balsara, N. P. Polymer Electrolytes. *Annu. Rev. Mater. Res.* **2013**, *43*, 503–525.

(48) Ketkar, P. M.; Shen, K. H.; Hall, L. M.; Epps, T. H. Charging toward Improved Lithium-Ion Polymer Electrolytes: Exploiting Synergistic Experimental and Computational Approaches to Facilitate Materials Design. *Mol. Syst. Des. Eng.* **2019**, *4*, 223–238.

(49) Webb, M. A.; Jung, Y.; Pesko, D. M.; Savoie, B. M.; Yamamoto, U.; Coates, G. W.; Balsara, N. P.; Wang, Z. G.; Miller, T. F. Systematic Computational and Experimental Investigation of Lithium-

Ion Transport Mechanisms in Polyester-Based Polymer Electrolytes. *ACS Cent. Sci.* **2015**, *1*, 198–205.

(50) Webb, M. A.; Savoie, B. M.; Wang, Z. G.; Miller, T. F. Chemically Specific Dynamic Bond Percolation Model for Ion Transport in Polymer Electrolytes. *Macromolecules* **2015**, *48*, 7346–7358.

(51) Jackson, N. E.; Savoie, B. M.; Chen, L. X.; Ratner, M. A. A Simple Index for Characterizing Charge Transport in Molecular Materials. *J. Phys. Chem. Lett.* **2015**, *6*, 1018–1021.

Recommended by ACS

Mismatch in Nematic Interactions Leads to Composition-Dependent Crystal Nucleation in Polymer Blends

Wenlin Zhang and Lingyi Zou

MARCH 07, 2023

MACROMOLECULES

READ 

Microphase Separation in Neutral Homopolymer Blends Induced by Salt-Doping

Xian Kong and Jian Qin

DECEMBER 29, 2022

MACROMOLECULES

READ 

Orientational Wetting and Topological Transitions in Confined Solutions of Semiflexible Polymers

Maxime M. C. Tortora and Daniel Jost

FEBRUARY 13, 2023

MACROMOLECULES

READ 

Interrogating Polymorphism in Conjugated Poly(thieno)thiophene Thin Films for Field-Effect Transistors

Qingqing Zhao, Juan Peng, *et al.*

DECEMBER 30, 2022

MACROMOLECULES

READ 

Get More Suggestions >